Nanoscale

Accepted Manuscript

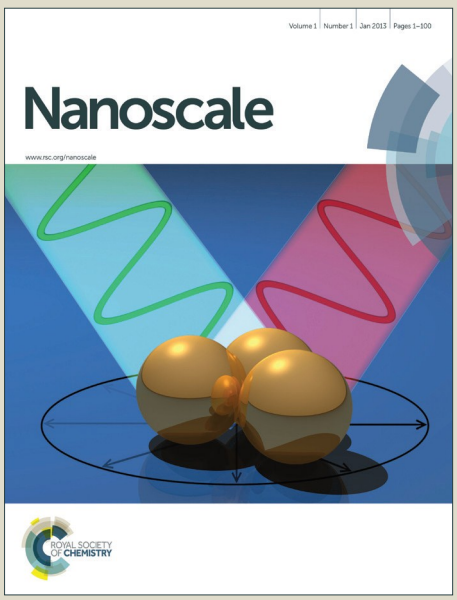

ROYAL SOCIETY OF CHEMISTRY

www.rsc.org/nanoscale

potential as excellent theranostic nanoprobes in cancers.[21-23] Due to the ultra-large surface area and pore volume, yolk-shell nanomaterial was considered as a promising nanocarrier in drug delivery, by which the high loading efficiency could be achieved. Currently, many efforts have been taken by developing different yolk-shell nanoparticles,[24-26] especially solid silica@mesoporous silica yolk-shell nanostructure.[27] Moreover, to integrate imaging and therapy, different functional core@mesoporous silica yolk-shell nanoparticles were designed and investigated for simultaneous imaging and treatment in tumors, also for quantitative monitor of drug release.[28-34] Due to the excellent imaging performance, yolk-shell nanoparticles with UCL nanoparticle as core have attracted great attention.[35-40] Very recently, Shi *et al.* reported a series of Gd-based UCL yolk-shell nanoparticles for the delivery of drugs, radiosensitizer or photosensitizer to achieve chemotherapy, radiotherapy and photodynamic therapy.[38-40] Moreover, the previous reports indicated the *in vivo* biosafety of UCL nanomaterials, also including Gd-based UCL yolk-shell nanocomposites. [37, 39, 45, 46] However, Gd-based UCL yolk-shell delivery system was still not reported as theranostic nanoprobes to overcome MDR in cancers. Therefore, it could be believed that yolk-shell nanomaterial will be an excellent candidate as a multifunctional delivery system, especially for diagnosis and visualized treatment in drug resistant cancers.

Here, we synthesized DOX-loaded multifunctional $NaYF_4$:Yb/Er@$NaGdF_4$- mesoporous silica nanoparticles with yolk-shell structure as delivery system for simultaneous UCL, magnetic resonance (MR) imaging and enhanced chemotherapy in drug resistant breast cancer. The designed delivery system showed a large pore volume, a high loading capability and an excellent dual-modal imaging performance of UCL and MR. By comparing drug sensitive (MCF-7) and drug resistant (MCF-7/ADR) breast cancer cells, the as-prepared delivery system could greatly improve the uptake and enhanced the chemotherapy efficacy of MCF-7/ADR cells. Our work showed that the synthesized Gd-based UCL nanocarrier with yolk-shell structure had potential applications in dual-modal imaging and visualized treatment to overcome MDR in breast cancer.

Results and discussion

The synthesis of DOX-loaded yolk-shell Gd-based upconversion nanocarriers was shown in Fig. 1. The hexagonal-phase core-shell UCNPs were first prepared *via* a seeded growth approach, and then coated with a dense layer of silica by a microemulsion strategy. In the presence of CTAB as the template, a mesoporous silica layer was deposited onto the surface of UCNPs@SiO_2 by an aqueous phase regrowth method. Subsequently, the inner silica was selectively etched out, and the final products, UCNPs-yolk-shell nanoparticles with UCNPs located within the outer mesoporous silica layer, and interstitial hollow spaces were obtained. The huge loading capacity of large pore volume for DOX can be used for chemotherapies, further better capability in overcoming MDR. At the same time, the intrinsic property of Gd-based upconversion can be used for UCL/MR imaging, thus achieved the purpose of dual-modal imaging and visualized enhanced chemotherapy to overcome MDR.

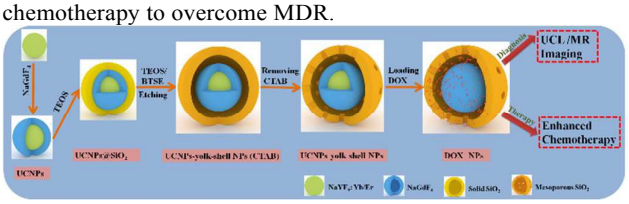

Fig.1 Synthesis scheme of DOX-loaded yolk-shell Gd-based upconversion nanocarriers for dual-modal UCL/MR imaging and enhanced chemotherapy to overcome MDR in breast cancer.

Synthesis and Characterization of UCNPs-Yolk-Shell Nanoparticles

To make sure the Gd-based upconversion nanocarriers with yolk-shell structure were successfully fabricated, the morphologies of different nanoparticles were characterized, respectively. Fig. 2(a) and (b) showed the TEM images of $NaYF_4$:Yb/Er UCNPs and $NaYF_4$:Yb/Er@$NaGdF_4$ UCNPs, in which their sizes were about 35 nm and 45 nm, respectively. By a reverse microemulsion method, a layer of dense silica about 12 nm thick was coated onto the surface of $NaYF_4$:Yb/Er@$NaGdF_4$ UCNPs to form UCNPs@SiO_2 NPs, as shown in Fig. 2(c). In the presence of CTAB as the template, a mesoporous silica shell was deposited onto the surface of UCNPs@SiO_2 to form UCNPs@SiO_2@mSiO_2, as seen in Fig. 2(d).Then following a typical "surface-protected hot water etching" strategy, the inner dense silica layer can be etched out. As seen in Fig. 2(e), UCNPs-yolk-shell (CTAB) NPs with spherical morphology were gotten. After the CTAB of outer mesoporous silica shell were etched by HCl, the UCNPs-yolk-shell nanoparticles were successfully fabricated, as shown in Fig. 2(f).

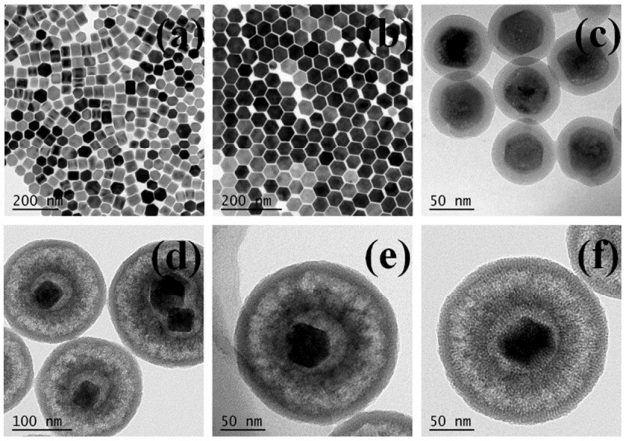

Fig. 2 TEM images of different nanoparticles. (a) $NaYF_4$: Yb/Er UCNPs; (b) $NaYF_4$:Yb/Er@$NaGdF_4$ UCNPs; (c) UCNPs@SiO_2 NPs; (d) UCNPs@SiO_2 @mSiO_2 NPs; (e) UCNPs-yolk-shell (CTAB) NPs; and (f) UCNPs-yolk-shell nanoparticles.

To further investigate their applications in imaging and treatment, the physiochemical properties of nanoparticles were firstly characterized. Firstly, the crystalline structure of nanoparticles was determined by XRD technique. Fig. 3(a)

showed the XRD patterns of different nanoparticles, in which the as-prepared $NaYF_4$:Yb/Er and $NaYF_4$:Yb/Er@$NaGdF_4$ were both hexagonal structure, and the broad band (at about 2θ=22°) of UCNPs-yolk-shell nanoparticles suggested the successful coating of silica on the surface of $NaYF_4$:Yb/Er@$NaGdF_4$ nanoparticles. Secondly, the hydrodynamic sizes of different nanoparticles were measured by DLS, as shown in Fig. 3(b). It could be found that the sizes of non-yolk-shell nanoparticles were between 130-170 nm. After the formation of yolk-shell structure, the size of nanoparticles could increase to be about 240-265 nm. Compared with TEM results, the size increase could attribute to the hydrodynamic interaction.

Under the excitation of a 980 nm laser, the UCL performance of different nanoparticles was evaluated by measuring their UCL spectra. As shown in Fig. 3(c), the UCL intensity of $NaYF_4$:Yb/Er@$NaGdF_4$ had greatly enhanced, compared with that of $NaYF_4$:Yb/Er, which could be attributed to the protection of $NaGdF_4$ shell. Due to the coating of silica layer, the UCL intensity of UCNPs-yolk-shell nanoparticles shows a little decrease, but it was still much better than that of $NaYF_4$:Yb/Er. Moreover, Fig. 3(d) showed that the Brunauer–Emmett–Teller (BET) surface area and the total pore volume were about 1100.7 m^2g^{-1} and 1.06 cm^3g^{-1}, respectively, in which the isotherm could be classified as a type-IV isotherm, indicating the presence of textural mesopores. The pore sizes was calculated to be dual mode with 2.23nm and 4.01nm using the Barrett-Joiner-Halenda (BJH) method, as shown in the inset of Fig. 3(d). Due to the large pore volume and mesoporous outer shell of UCNPs@yolk shell NPs, DOX could be easily loaded inside the hollow inner spaces through the outer mesoporous silica shell for high-efficiency drug delivery.

In order to evaluate the loading and controlled release abilities of UCNPs@yolk shell NPs, the loading efficiency and release performance of DOX were measured, respectively. Fig. 3(e) gave the standard curves of free DOX, and then the loading efficiency was calculated to be about 8.74 %, which was determined by measuring absorption peak of DOX at 480 nm. Furthermore, in PBS buffer solutions with the pH of 7.4 and 5.0, the DOX release properties of DOX-UCNPs@yolk shell NPs were investigated. As show in Fig. 3(f), the accumulative release of DOX at the pH of 5.0 could reached 58.3 % and 71.9 % after 24 h and 108 h, respectively. However, they were only 18.6% and 27.6 % at the pH of 7.4, which indicated the pH-responsive mode of the designed delivery system. Therefore, considering the acidic environment of tumor tissue, the high loading capacity of DOX and a sustained drug release property made the DOX- UCNPs@yolk shell NPs applicable for cancer therapy.

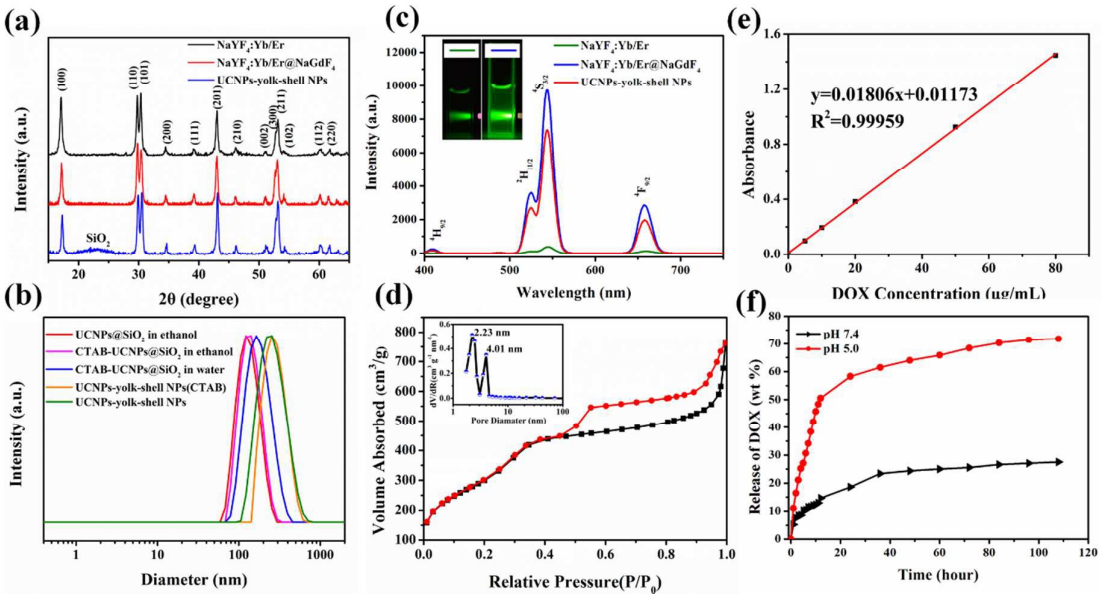

Fig. 3 Physicochemical performance characterization of the as-prepared nanoparticles. (a) XRD patterns of different nanoparticles; (b) DLS curves of different nanoparticles; (c) UCL spectra of different nanoparticles under excitation of a 980 nm laser; (d) N_2 adsorption–desorption isotherms of UCNPs-yolk-shell nanoparticles (the inset showed the size distribution of mesopores); (e) The standard curves of free DOX for the measurement of DOX loading efficiency; (f) DOX release curves of DOX-UCNPs-yolk-shell nanoparticles in PBS buffer under the pH of 7.4 and 5.0.

MR and UCL Performance

It was well known that paramagnetic Gd^{3+} with seven unpaired electrons and weak longitudinal relaxivity has been proved to be an excellent T_1-weighted MRI contrast agent.[43, 44] To investigate the MR performance of UCNPs-yolk-shell nanoparticles, the MR relaxivity and the MR imaging of UCNPs-yolk-shell nanoparticles were evaluated. As shown in Fig. 4(a) and (b), a good linear relationship was observed between Gd concentrations and the corresponding $1/T_1$ ($1/T_2$) values, Based on the slope, the longitudinal and the transverse relaxivity of UCNPs-yolk-shell nanoparticles were calculated to be r_1=1.04 and r_2=3.89 mM^{-1} s^{-1}, respectively. Fig. 4 (c) showed the T_1- and T_2-weighted MRI images of UCNPs-yolk-

shell nanoparticles with different concentrations from 0.2 to 1.0 mM, in which T_1-weighted signals got brighter and brighter by increasing the concentration of UCNPs-yolk-shell nanoparticles, but T_2-weighted signals did not nearly changed, indicating the as-prepared UCNPs-yolk-shell nanoparticles could serve as an effective T_1-weighted MRI contrast agent.

Moreover, the UCL imaging of the as-prepared UCNPs-yolk-shell nanoparticles and their incubation with MCF-7, MCF-7/ADR cells were also observed, in which the concentration of UCNPs-yolk-shell nanoparticles changed from 0.2 to 1.0 mM. By centrifugation, the precipitated nanoparticles (10000 rpm) and MCF-7 (1000 rpm), MCF-7/ADR (1000 rpm) cells incubated with nanoparticles were irradiated by a 980 nm laser. As shown in Fig. 4(d), the green fluorescence of UCNPs-yolk-shell nanoparticles got brighter by increasing nanoparticle concentration. Especially, in MCF-7 and MCF-7/ADR cell samples, the UCL was also observed, which indicated the as-prepared UCNPs-yolk-shell nanoparticles could be greatly uptaken by MCF-7 and MCF-7/ADR cells.

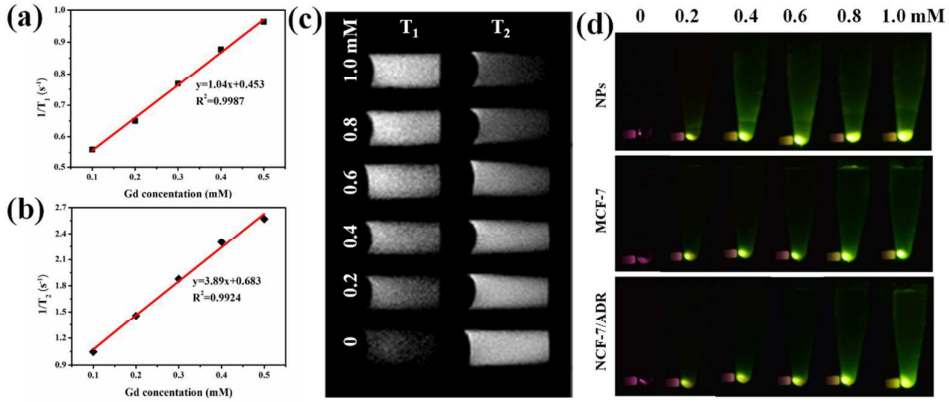

Fig. 4 MR relaxivities, MR imaging and UCL imaging of UCNPs-yolk-shell nanoparticles. (a)-(b) Longitudinal (r_1) and transverse (r_2) relaxivity curves of UCNPs-yolk-shell nanoparticles; (c) T_1- and T_2-weighted MR images of UCNPs-yolk-shell nanoparticles with different Gd concentrations, respectively; (d) UCL images of UCNPs-yolk-shell nanoparticles and MCF-7, MCF-7/ADR cells incubated with UCNPs-yolk-shell nanoparticles under different concentrations irradiated by a 980 nm laser, respectively.

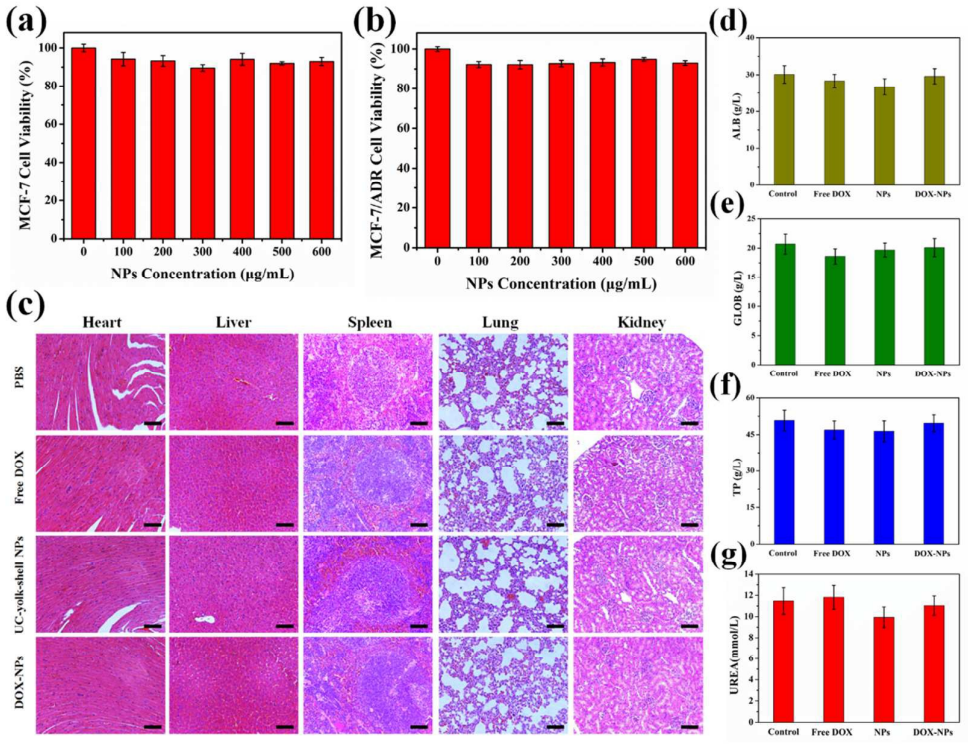

Fig. 5 In vitro and in vivo biocompatibility characterization of UCNPs-yolk-shell nanoparticles. (a) and (b) Viabilities of MCF-7 and MCF-7/ADR cells incubated with UCNPs-yolk-shell nanoparticles, respectively; (c) H&E staining images of major organs (heart ,liver, spleen, lung and kidney) of healthy

nude mice injected with free DOX, UCNPs-yolk-shell nanoparticles and DOX NPs *via* the tail vein, respectively; (d)-(g) Blood biochemistry analysis (ALB,GLOB,TP and UREA) of healthy nude mice injected with free DOX, UCNPs-yolk-shell nanoparticles and DOX NPs *via* the tail vein, respectively.

In Vitro and *in Vivo* Biocompatibility

As a drug delivery system, it was important of good biocompatibility *in vitro* and *in vivo*. The cytotoxicity of the UCNPs-yolk-shell nanoparticles was evaluated *via* MTT assay method, Fig. 5(a) and (b) showed the viabilities of MCF-7 and MCF-7/ADR cells incubated with UCNPs-yolk-shell nanoparticles for 24 h, respectively. It could be seen that the viabilities were both higher than 90 % for MCF-7 and MCF-7/ADR cells, respectively, which indicated the excellent *in vitro* biocompatibility of the as-prepared UCNPs-yolk-shell nanoparticles.

To evaluate the *in vivo* biocompatibility of the drug delivery system, the healthy nude mice were injected with PBS, free DOX, UCNPs-yolk-shell nanoparticles and DOX- NPs *via* tail vein, respectively. After three weeks, the *in vivo* toxicity was investigated by blood biochemical assays and H&E staining analysis of major organs (heart, liver, spleen, lung and kidney). As seen in Fig. 5(c) about H&E staining images of major organs, no noticeable tissue damage and obvious change in morphology were observed in all organs from the groups of UCNPs-yolk-shell nanoparticles and DOX- NPs, compared with that of PBS group. Moreover, the organs from the group of free DOX were also normal at this injection dose. Furthermore, using blood biochemical assays, the liver and kidney functions of healthy nude mice were evaluated, in which the nude mice were injected with PBS, free DOX, UCNPs-yolk-shell nanoparticles and DOX-NPs *via* tail vein, respectively. As shown in Fig.5 (d)-(g), the liver function markers consisting ALB (albumin), GLOB (globulin) and TP (total protein) appeared to be normal, and the kidney function marker of UREA (urea), was also within the reference normal range, compared with that of PBS group. The *in vitro* and *in vivo* results suggested that the as-prepared NPs have excellent biocompatibility, and have potential biological applications with few side effects.

Cellular Uptake

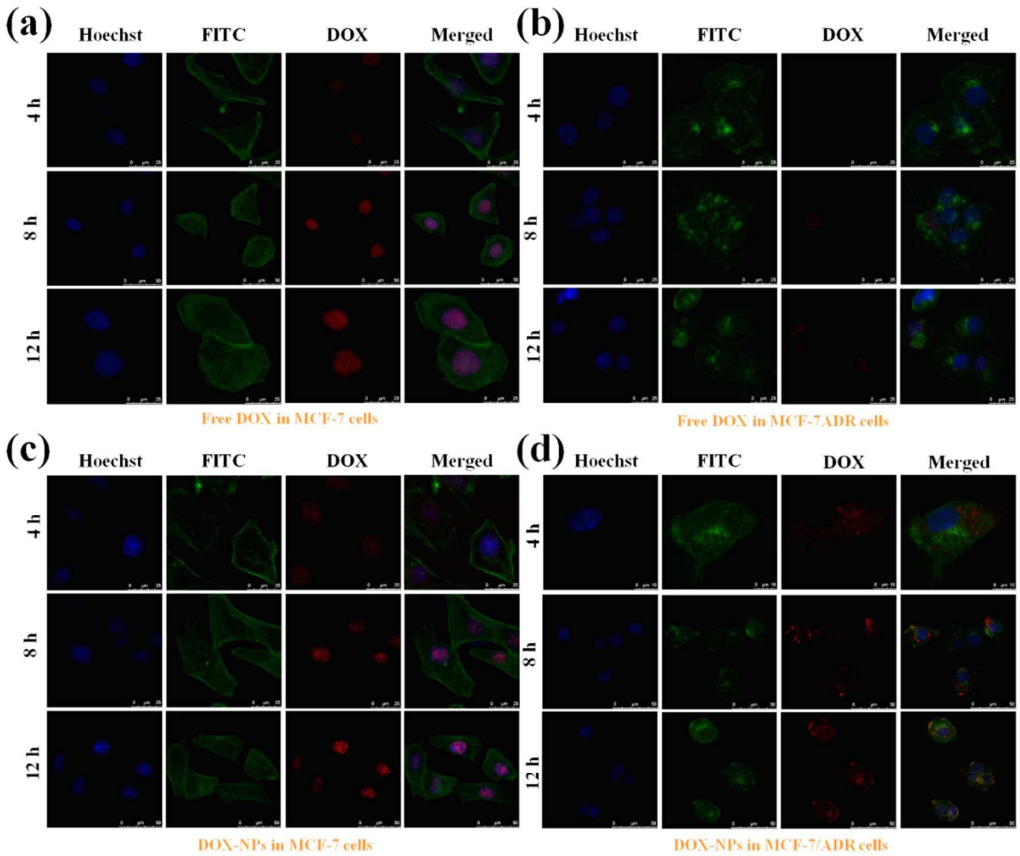

Fig. 6 Laser confocal microscopy images of MCF-7 and MCF-7/ADR cells. (a) and (b) MCF-7 and MCF-7/ADR cells incubated with free DOX, respectively (the incubation time was 4 h, 8 h and 12 h); (c) and (d) MCF-7 and MCF-7/ADR cells incubated with DOX-NPs (the incubation time was 4 h, 8 h and 12 h, respectively).

Nanoscale

PAPER

It was well known that the DOX could not have antitumor effects before their release in nucleus. To further confirm cellular uptake capability and verify the location of UCNPs-yolk-shell nanoparticles in MCF-7 and MCF-7/ADR cells, CLSM was used to observe the process of cellular uptake. Fig. 6(a) and (b) showed the CLSM images of MCF-7 and MCF-7/ADR cells incubated with free DOX at different time, respectively. It could be seen that DOX could easily enter into nucleus of MCF-7 cells, but could hardly be uptaken by MCF-7/ADR cells. However, after DOX-UCNPs-yolk-shell nanoparticles were incubated with MCF-7 and MCF-7/ADR cells at different time, it was found that DOX could be accumulated in MCF-7 cells, also in drug resistant MCF-7/ADR cells. As shown in Fig. 6(c) and (d), the accumulation and release of DOX in MCF-7/ADR cells were obviously enhanced by increasing incubation time, which demonstrated the as-prepared DOX-UCNPs-yolk-shell nanoparticles was good candidate as delivery system and had potential applications in overcoming MDR of breast cancer.

Furthermore, the statistical analysis of cellular uptake was also characterized using flow cytometry by measuring the fluorescence intensity of DOX. Fig. 7 showed flow cytometry curves of MCF-7 and MCF-7/ADR cells incubated with different samples, respectively. In Fig. 7(a), the fluorescence intensity of DOX did not have significant difference in the samples of free DOX and DOX-UCNPs-yolk-shell nanoparticles, indicating that both free DOX and DOX-UCNPs-yolk-shell nanoparticles could easily be uptaken by MCF-7 cells. However, for MCF-7/ADR cells, significant difference was observed between free DOX and DOX-UCNPs-yolk-shell nanoparticles, in which the fluorescent intensity of DOX-UCNPs-yolk-shell nanoparticles was about 10 times stronger than that of free DOX, indicating an increasing accumulation of DOX in MCF-7/ADR cells in the sample of DOX-UCNPs-yolk-shell nanoparticles. These results were also consistent with the cellular uptake process observed by CLSM.

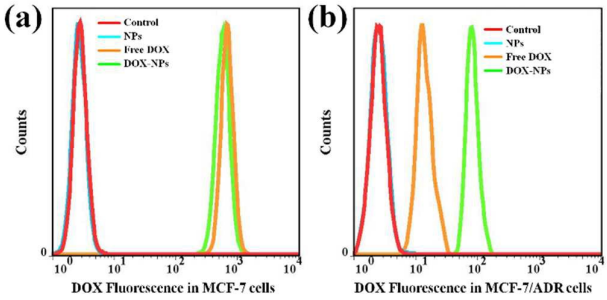

Fig. 7 Flow cytometry curves of MCF-7 and MCF-7/ADR cells incubated with NPs, free DOX and DOX-NPs by measuring DOX fluorescence, respectively. (a) MCF-7 cells; (b) MCF-7/ADR cells.

Alternatively, the element distribution and location of different nanoparticles in MCF-7 and MCF-7/ADR cell were also directly observed using the X-ray fluorescence microscope (XFM) based on free-staining. Fig. 8 showed the XFM images of MCF-7 and MCF-7/ADR cells incubated with UCNPs-yolk-shell nanoparticles and DOX-UCNPs-yolk-shell nanoparticles, respectively, in which the element of S was used to sketch cells and the elements of Gd and Yb were used to sketch nanoparticles. It was obviously observed that the elements of Gd and Yb were accumulated in MCF-7 and MCF-7/ADR cells incubated with nanoparticles, compared with that of cells in control. The XFM characterization directly demonstrated the strong capability of cellular uptake of the as-prepared nanoparticles, which was also consistent with the results in CLSM and flow cytometry.

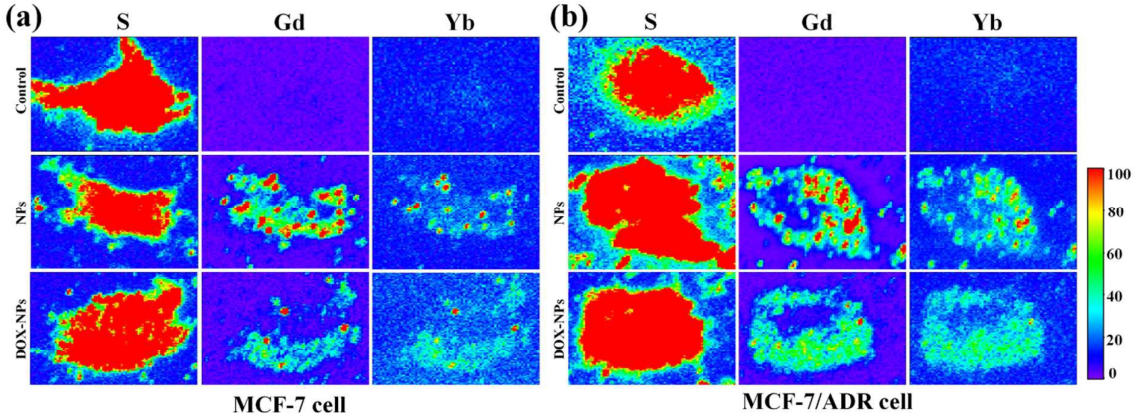

Fig. 8 XFM images of MCF-7 and MCF-7/ADR cells incubated with NPs and DOX-NPs by measuring element fluorescence, respectively. (a) MCF-7 cell; (b) MCF-7/ADR cell.

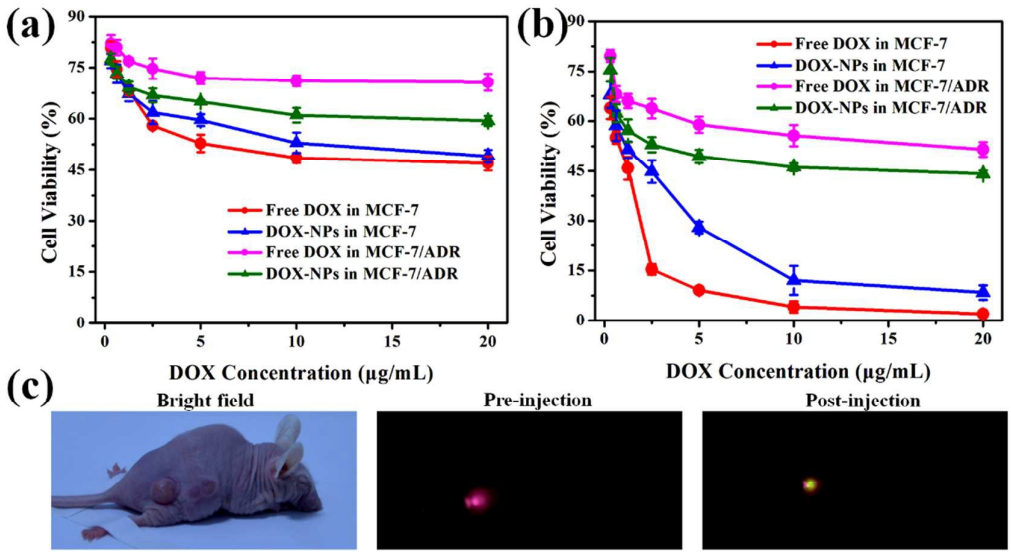

Fig. 9 In vitro chemotherapy efficacy and in vivo UCL imaging. (a) Viabilities of MCF-7 and MCF-7/ADR cells incubated with free DOX and DOX-NPs for 24 h, respectively; (b) Viabilities of MCF-7 and MCF-7/ADR cells incubated with free DOX and DOX-NPs for 24 h, respectively; (c) In vivo UCL images of MCF-7/ADR bearing tumors injected with DOX-NPs under a 980 nm laser.

In Vitro Chemotherapy and *in Vivo* UCL imaging

In order to investigate the chemotherapy performance of DOX-UCNPs-yolk-shell nanoparticles in MCF-7/ADR cells, the viabilities of MCF-7 and MCF-7/ADR cells incubated with free DOX and DOX-UCNPs-yolk-shell nanoparticles for 24 h and 48 h were tested by MTT assay method, respectively. As presented in Fig. 9(a), the viabilities of MCF-7 cells incubated with free DOX and DOX-UCNPs-yolk-shell nanoparticles were similar, decreased to about 47.0% and 49.1%, even higher efficacy in the sample of free DOX. However, for MCF-7/ADR cells, the viabilities decreased to about 70.7% and 59.4%, in which free DOX had bad efficacy. Similarly in Fig. 9(b), after they were incubated for 48 h, all the MCF-7 cells were nearly killed in the sample of free DOX and DOX-UCNPs-yolk-shell nanoparticles, in which the viabilities were 4.1% and 12.1%, respectively. However, free DOX only decreased the viability of MCF-7/ADR cells to about 51.6%, but 44.2% for the sample of DOX-UCNPs-yolk-shell nanoparticles. Therefore, it could be concluded that in drug resistant MCF-7/ADR cells, the as-prepared delivery system of UCNPs-yolk-shell nanoparticles was more effective than that of free DOX, but free DOX was better in drug sensitive MCF-7 cells. Furthermore, in Fig. 9(c), the *in vivo* UCL imaging of the UCNPs-yolk-shell nanoparticles indicated the as-prepared UCNPs-yolk-shell nanoparticles could simultaneously act as NIR-responsive UCL nanoprobes for tumors imaging in deep-tissue *in vivo*.

Experimental Section

Materials

Gadolinium oxide (Gd_2O_3, 99.9%), yttrium oxide (Y_2O_3, 99.9%), ytterbium oxide (Yb_2O_3, 99.9%), erbium oxide (Er_2O_3, 99.99%), ammonium fluoridenitric (NH_4F, 98%), sodium hydroxide (NaOH, 99.99%), methanol (analytical grade, 99.5%), ammonium hydroxide ($NH_3 \cdot H_2O$, 25-28%), tetraethyl orthosilicate (TEOS, 99.9%), cyclohexane (analytical grade, 99.5%), cetyl trimethyl ammonium bromide (CTAB, 99%) and dimethyl sulfoxide (DMSO, analytical grade) were purchased from Aladdin Industrial Inc. (Shanghai, China). Oleic acid (90%) and 1-octadecene (90%) were purchased from Alfa Aesar (Shanghai, China). Hydrochloric acid (HCl, analytical grade), absolute ethanol (analytical grade), 3-(4,5-di-methylthiazol-2-yl)-2,5-diphenyltetrazolium bromide (MTT), and doxorubicin (DOX) were purchased from Sino-pharm Chemical Reagent Co., Ltd. (Shanghai, China). 1,2-Bis(triethoxysilyl)ethane (BTSE) and Igepal CO-520 were purchased from Sigma–Aldrich Co. LLC. (China). Dulbecco's modified Eagle's medium (DMEM), fetal bovine serum (FBS), penicillin and streptomycin were purchased from Invitrogen (USA). All reagents were used as received without further purification. Milli-Q water (18.2 $M\Omega \cdot cm^{-1}$) was used in all experiments.

Synthesis of Yolk-Shell Nanoparticles

Synthesis of β-$NaYF_4$:Yb/Er@$NaGdF_4$ UCNPs. The oleic acid stabilized $NaYF_4$:Yb/Er@$NaGdF_4$ upconversion nanoparticles (UCNPs) were prepared following the previously reported method.[41] To obtain rare earth (RE) chlorides, rare-earth oxides were dissolved in excess hydrochloric acid solution and the solution was heated to evaporate the water completely. Then, $NaYF_4$:Yb/Er UCNPs were prepared following the previously reported method. At First, 1.0 mmol $RECl_3$ (RE=Y, Yb or Er; Y:Yb:Er=0.78 mmol: 0.2 mmol: 0.02 mmol) was mixed with 8 mL of oleic

acid and 15 mL of 1-octadecene in a 100 mL flask and then heated to 160 °C under an argon atmosphere for 30 min to form a homogeneous solution. After the solution was cooled to room temperature, 10 mL methanol containing NaOH (2.5 mmol) and NH_4F (4.0 mmol) were slowly added into the flask and the solution was kept at 50 °C for 30 min. Subsequently, the solution was heated to 100 °C and degassed for 10 min in order to remove methanol. Then the solution was heated to 300 °C and maintained for 1 h under argon atmosphere. The as-prepared $NaYF_4$:Yb/Er UCNPs were collected by centrifugation (10000 rpm for 10 min) and washed with ethanol/cyclohexane for three times. Finally, the $NaYF_4$:Yb/Er UCNPs were re-dispersed into 6 mL cyclohexane.

Later, β-$NaYF_4$:Yb/Er@$NaGdF_4$ UCNPs were prepared. Briefly, $GdCl_3$ (1.0 mmol) was mixed with 8 mL of oleic acid and 15 mL of 1-octadecene in a 100 mL flask and then heated to 160 °C under an argon atmosphere for 30 min to form a homogeneous solution. After the solution was cooled down to 120 °C, the as-prepared $NaYF_4$:Yb/Er UCNPs in 6 mL cyclohexane were added into the flask and kept 120 °C for 10 min to remove cyclohexane. The below process was the same as that of $NaYF_4$:Yb/Er UCNPs. Finally, the as-prepared $NaYF_4$:Yb/Er@$NaGdF_4$ UCNPs were collected by centrifugation (10000 rpm for 10 min) and washed with ethanol/cyclohexane for three times.

Synthesis of UCNPs@SiO_2 Nanoparticles. The SiO_2 shell was coated on $NaYF_4$:Yb/Er@$NaGdF_4$ UCNPs through a reverse microemulsion method. Typically, 2 mL of Igepal CO-520 in 5 mL of cyclohexane and 15 mg of UCNPs in 20 mL of cyclohexane were sonicated for 10 min, respectively. Then, CO-520 cyclohexane solution was added into the UCNPs cyclohexane solution, and the mixed solution was sonicated for another 10 min. After that, 400 μL of $NH_3 \cdot H_2O$ were added and the system was sealed and sonicated for 20 min until a transparent emulsion was formed. Subsequently, 200 μL of TEOS was injected into the system at a rate of 40 μL/10 min. The solution was sealed and stirred for 48 h and the product was precipitated with ethanol/water (V:V=1:1). Finally, the resultant UCNPs@SiO_2 nanoparticles were collected by centrifugation (10000 rpm for 10 min) and washed with ethanol for three times.

Synthesis of UCNPs-Yolk-Shell Nanoparticles. The as-prepared UCNPs@SiO_2 nanoparticles were dispersed into 25 mL of absolute ethanol containing 200 mg of CTAB, and the solution was stirred for 24 h at room temperature. Then the CTAB-UCNPs@SiO_2 nanoparticles were collected by centrifugation (10000 rpm for 10 min) and washed with ethanol for three times. The UCNPs-yolk-shell nanoparticles were prepared by the previously reported method.[42] Briefly, CTAB-UCNPs@SiO_2 NPs were dispersed into 33.5 mL of absolute ethanol and 11.5 mL of Milli-Q water, which contained 160 mg of CTAB and 400 μL of $NH_3 \cdot H_2O$, and was heated to 35 °C. Subsequently, 100 μL of TEOS and 50 μL of BTSE in 1.0 mL of absolute ethanol were rapidly added under vigorous magnetic stirring, and the reaction was kept for 20 h at 35 °C. Afterwards, the product was collected by centrifugation (10000 rpm for 10 min) and washed with absolute ethanol for three times, and then dispersed in 30 mL of Milli-Q water at 70 °C for 24 h. The resultant UCNPs-yolk-shell (CTAB) NPs were collected by centrifugation (8000 rpm for 10 min) and washed with absolute ethanol for three times.

To remove the pore-generating template (CTAB), the product was dispersed into 50 mL of absolute ethanol and 10 mL of Milli-Q water containing 20 μL of HCl, and the solution was stirred at 60 °C for 3 h. Then the nanoparticles were collected by centrifugation (8000 rpm for 10 min) and washed with absolute ethanol for twice. The resultant UCNPs-yolk-shell nanoparticles were finally gotten after the extraction process was repeated for three times.

Characterization

Transmission electron microscopy (TEM) images were obtained on a JEOL-2100 transmission electron microscope operating at 200 kV. Powers X-ray diffraction (XRD) measurements were performed on a D8 Focus diffractometer (Bruker) with use of Cu-Ka radiation, operating at 40 kV and 40 mA. Dynamic light scattering (DLS) experiments were conducted on Zeta-sizer Nanoseries (Nano-ZS, Malvern Instruments). UCL spectra were recorded on a F-4600 fluorescence spectrophotometer (Hitachi, Japan), using an external 0 to 2 W adjustable 980 nm semiconductor laser (HI-Tech Optoelectronics Co., Ltd.) as the excitation source. Inductively coupled plasma optical emission spectrometry (ICP-OES) were performed with an Optima 2100 instrument from Perkin Elmer. The UV–Vis adsorption spectra were measured on a UV-vis spectrophotometer (Lambda 950, Perkin Elmer, USA). Nitrogen adsorption/desorption analysis was measured by the ASAP 2020 M apparatus (Micromeritics, USA). The specific surface area was determined by the Brunauer–Emmett–Teller (BET) method and the pore volume was obtained from the t-plot method.

Drug Loading and Release

10 mg of UCNPs-yolk-shell nanoparticles were mixed with 4 mL of DOX solution in PBS (0.25 mg/mL). After stirring for 24 h under dark condition, the DOX-loaded UCNPs-yolk-shell nanoparticles (DOX-NPs) were collected by centrifugation at 13000 rpm for 15 min. To evaluate the DOX loading capacity, the supernatant was collected and the residual DOX was measured by a UV-vis spectrophotometer at a wavelength of 480 nm. Finally, the DOX loading capacity and efficiency were calculated, respectively.

To investigate the drug release behavior of DOX-NPs, the prepared DOX-NPs were dispersed into 2 mL of PBS with pH=7.4 and 5.0, and then transferred into dialysis bags (3500 Da), respectively. Then the dialysis bags were placed into the beakers containing 48 mL of PBS with pH=7.4 and 5.0, and the solutions were gently stirred under dark condition. At predetermined time intervals, 1 mL of PBS was taken out from each beaker for UV-vis measurement to determine the amount of released DOX. Simultaneously, 1 mL of fresh PBS (pH = 7.4 or 5.0) was returned to original solution.

MR and UCL Performance

The MR relaxivity and MR imaging of UCNPs-yolk-shell nanoparticles were measured on a MesoMR23-060H-1 MR instrument with a magnetic field of 0.5 T (Niumag, Shanghai of China). The relaxation times (T_1, T_2) of UCNPs-yolk-shell nanoparticles in Milli-Q water with various Gd concentrations (0.1, 0.2, 0.3, 0.4 and 0.5 mM) were measured, and then the longitudinal (r_1) and the transverse (r_2) relaxivities were calculated from the slope of inverse relaxation times ($1/T_1$ and $1/T_2$) plotted against different Gd concentrations. Moreover, MR imaging were also performed with various Gd concentrations (0, 0.2, 0.4, 0.6, 0.8, and 1.0 mM).

The UCL imaging of the as-prepared UCNPs-yolk-shell nanoparticles and MCF-7, MCF-7/ADR cells incubated with UCNPs-yolk-shell nanoparticles were measured under excitation of a 980 nm laser (λ=980 nm, power density=0.5 W/cm^2). Briefly, 2 mL of cells (MCF-7 and MCF-7/ADR) were seeded in a 6-well plate at the density of 1×10^5 cells/mL and incubated for 24 h. Then those cells were incubated with UCNPs-yolk-shell nanoparticles at a series of Gd concentrations from 0 to 1.0 mM for another 24 h. After that the cells were washed with PBS, and collected by centrifugation at 1000 rpm for 5 min, the same Gd concentrations of UCNPs-yolk-shell nanoparticles were collected by centrifugation at 10000 rpm as the control. Finally the UCL imaging of each sample was recorded by a digital camera under excitation of a 980 nm laser, respectively.

In Vitro and *In Vivo* Biocompatibility

Human breast cancer MCF-7 cells and drug resistant MCF-7/ADR cells were cultured, respectively. To evaluate the *in vitro* cytotoxicity, MTT assay was performed on the MCF-7 and MCF-7/ADR cells. Briefly, 100 μL of cells (MCF-7 and MCF-7/ADR) were seeded in a 96-well plate at the density of 1×10^5 cells/mL and incubated for 24 h. Serial concentrations of UCNPs-yolk-shell nanoparticles in 100 μL of the culture medium were added and incubated for another 24 h. The final concentrations of the nanoparticles were 100, 200, 300, 400, 500 and 600 μg/mL, respectively. 10 μL of MTT (5 mg/mL) was added to each well. After additional 4 h incubation, the medium and MTT were removed, and the MTT-formazan crystals in each well were dissolved in 100 μL of DMSO. The absorbance of the suspension was recorded by a microplate reader (iMark 168-1130, Bio-rad, USA) at a wavelength of 550 nm.

For *in vivo* toxicity, 12 healthy female Balb/c (nu/nu) nude mice (18-20 g, 4-6 weeks old) were divided into four groups (n=3) and intravenously injected by 100 μL of PBS, 100 μL of free DOX (100 μg/mL), 100 μL of UCNPs-yolk-shell nanoparticles (1045 μg/mL, in PBS) and 100 μL of DOX-NPs (1145 μg/mL, in PBS). After 3 weeks, the mice were drew blood for blood biochemical analysis, and the major organs (including heart, liver, spleen, lung, and kidney) were dissected for H&E staining and examined by an inverted fluorescence microscope (DMI3000, Leica). All the animal experiments were approved by the Institutional Animal Care and Use Committee of Jinling Hospital, the Animal Centre of Jinling Hospital.

Cellular Uptake and Evaluation

Confocal Laser Microscopy Observation. 2 mL of MCF-7 or MCF-7/ADR cells were seeded in a culture dish at a density of 5×10^4/mL or 7.5×10^4/mL, and incubated at 37 ° C in 5 % CO_2 for 24 h. Then, the culture medium was replaced by 2 mL of fresh culture which contained free DOX (20 μg/mL) or DOX-NPs (230 μg/mL, equivalent concentration of DOX with the free DOX). After being incubated for another 2, 4, 8 and 12 h, the cells were washed three times with PBS to remove the free nanoparticles and the free DOX. Then the cells were treated with FITC (5 μg/mL) and Hoechst (5 μg/mL) at room temperature to stain cytoskeleton and nucleus. Hoechst, FITC and DOX were excited at 405, 543 and 488 nm, respectively and the fluorescent images at emission wavelengths of 420-480, 500-540 and 600-660 nm were obtained by a confocal laser scanning microscope (CLSM) (TCS SP5 II, Leica).

Flow Cytometry Assay. MCF-7 and MCF-7/ADR cells were seeded in 6-well plates at a density of 2×10^5 and 3×10^5 cells and allowed to adhere at 37 °C for 24 h. Then the culture medium was removed and 2 mL of fresh culture medium (control group), UCNPs-yolk-shell nanoparticles in culture medium (210 μg/mL), free DOX in culture medium (20 μg/mL) and DOX-NPs in culture medium (230 μg/mL, equivalent concentration of DOX with the free DOX group) were added into the plates, respectively. After further 4.0 h incubation, the cells were washed three times with PBS to remove the free nanoparticles and the free DOX, collected by centrifugation at 1500 rpm for 5 min, and finally suspended in 1 mL ice-cold PBS for detecting the cellular accumulations of DOX by a flow cytometer (BD FACSCalibur, USA).

X-ray fluorescence Microscopy Analysis. MCF-7 and MCF-7/ADR cells were cultured on a Malay film which attached to the bottom of a 24-well plate. After 24 h, the cells were incubated with UCNPs-yolk shell NPs or DOX- UCNPs-yolk shell NPs for 2 h. Then the cells were washed with PBS for three times and fixed with 4% formaldehyde solution for 30 min. After that the elemental fluorescence mapping of cells was conducted at hard X-rays BL15U Beamline at the Shanghai Synchrotron Radiation Facility (Shanghai, China). The energy of the hard X-ray was 10 keV, and the beam spot was 0.5×0.5 μm^2. Finally, the element maps of S, Gd and Yb in MCF-7 and MCF-7/ADR cells were acquired and analyzed, respectively.

In Vitro Chemotherapy Efficacy

100 μL of MCF-7 and MCF-7/ADR cells were seeded in a 96-well plate at a density of 1×10^4 cells per well, and incubated at 37 ° C in 5 % CO_2 for 24 h. Then, 100 μL of free DOX, DOX-NPs at a series of concentration were added into each well, and the concentrations of DOX were 0, 1.25, 2.5, 5, 10, 20 g/mL, respectively. The cells were incubated at 37 °C in 5 % CO_2 for another 24 or 48 h, and finally the cell viabilities were measured by MTT assay method, respectively.

In Vivo Upconversion Luminescent Imaging

Tumor model of MCF-7/ADR was established and used for *in vivo* UCL imaging. When the MCF-7/ADR tumor grew to be about 30-50 mm^3, the nude mouse was injected with 30 μL of UCNPs-yolk-shell nanoparticles solution (4.0 mg/mL in PBS), and then the UCL image was acquired by a digital camera under the irradiation of a 980 nm laser at the tumor site.

Conclusions

In summary, we have developed a multifunctional nanocomposite based on DOX encapsulated $NaYF_4$:Yb/Er@$NaGdF_4$ yolk-shell delivery system. The nanocomposite provided a powerful platform for simultaneous imaging and therapy to overcome MDR in breast cancer. We have proved that the nanocomposites showed strong cellular uptake by drug resistant MCF-7/ADR cells, and the viability of MCF-7/ADR cells could decrease to about 44.2%, in which the chemotherapy efficacy was better than free DOX. Moreover, the nanocomposites showed strong UCL and MR imaging functions, which gave them the ability to act as imaging probes. As a result, the as-prepared DOX-UCNPs-yolk-shell nanoparticles had good biocompatibility and excellent theranostic performance, which could serve as a multifunctional nanoprobe for simultaneous dual-modal imaging of UCL/MR and enhanced chemotherapy to overcome MDR in breast cancer.

Acknowledgements

This work was supported by the National Key Basic Research Program of China (2014CB744504), the National Natural Science Foundation of China (U1332117 and U1432114), Science & Technology Department of Zhejiang Province (2015C31027), Science & Technology Bureau of Ningbo City (2015C50004 and 2015B11002), Key Breakthrough Program of Chinese Academy of Sciences (KGZD-EW-T06) and the Youth Innovation Promotion Association of Chinese Academy of Sciences (2015234). Furthermore, the authors also acknowledged Shanghai Synchrotron Radiation Facility at Line BL15U (No. h15sr0021) used for X-ray fluorescence imaging.

Notes and references

1 M. Ferrari, *Nat. Rev. Cancer*, 2005, **5**, 161-171.
2 M. M. Gottesman, T. Fojo and S. E. Bates, *Nat. Rev. Cancer*, 2002, **2**, 48-58.
3 G. Szakacs, J. K. Paterson, J. A. Ludwig, C. Booth-Genthe and M. M. Gottesman, *Nat. Rev. Drug Discov.*, 2006, **5**, 219-234.
4 B. A. Chabner and T. G. Roberts Jr, *Nat. Rev. Cancer*, 2005, **5**, 65-72.
5 Y. Chen, H. Chen and J. Shi, *Mol. Pharmaceut.*, 2014, **11**, 2495-2510.
6 L. Zeng, Y. Pan, S. Wang, X. Wang, X. Zhao, W. Ren, G. Lu and A. Wu, *ACS Appl. Mater. Inter.*, 2015, **7**, 16781-16791.
7 L. Zhang, L. Zeng, Y. Pan, S. Luo, W. Ren, A. Gong, X. Ma, H. Liang, G. Lu and A. Wu, *Biomaterials*, 2015, **44**, 82-90.
8 L. Zeng, L. Luo, Y. Pan, S. Luo, G. Lu and A. Wu, *Nanoscale*, 2015, **7**, 8946-8954.
9 L. Zeng, W. Ren, L. Xiang, J. Zheng, B. Chen and A. Wu, *Nanoscale*, 2013, **5**, 2107-2113.
10 Q. He, Y. Gao, L. Zhang, Z. Zhang, F. Gao, X. Ji, Y. Li and J. Shi, *Biomaterials*, 2011, **32**, 7711-7720.
11 L. Qiu, M. Qiao, Q. Chen, C. Tian, M. Long, M. Wang, Z. Li, W. Hu, G. Li, L. Cheng, L. Cheng, H. Hu, X. Zhao and D. Chen, *Biomaterials*, 2014, **35**, 9877-9887.
12 D. Kim, E. S. Lee, K. T. Oh, Z. G. Gao and Y. H. Bae, *Small*, 2008, **4**, 2043-2050.
13 A. Bhirde, A., B. Chikkaveeraiah, V., A. Srivatsan, A. Niu G. Jin, J., A. Kapoor, Z. Wang, S. Patel, V. Patel, A. Gorbach, M., R. Leapman, D., J. Gutkind, S., A. Walker, R. and X. Chen, *ACS Nano*, 2014, **8**, 4177-4189.
14 Y. Tian, X. Jiang, X. Chen, Z. Shao and W. Yang, *Adv. Mater.*, 2014, **26**, 7393-7398.
15 Y. Du, W. Ren, Y. Li, Q. Zhang, L. Zeng, C. Chi, A. Wu and J. Tian, *J. Mater. Chem. B*, 2015, **3**, 1518-1528.
16 W. Ren, L. Zeng, Z. Shen, L. Xiang, A. Gong, J. Zhang, C. Mao, A. Li, T. Paunesku, G. E. Woloschak, N. S. Hosmane and A. Wu, *RSC Adv.*, 2013, **3**, 20855.
17 J. N. Liu, W. Bu, L. M. Pan, S. Zhang, F. Chen, L. Zhou, K. L. Zhao, W. Peng and J. Shi, *Biomaterials*, 2012, **33**, 7282-7290.
18 G. Tian, X. Zheng, X. Zhang, W. Yin, J. Yu, D. Wang, Z. Zhang, X. Yang, Z. Gu and Y. Zhao, *Biomaterials*, 2015, **40**, 107-116.
19 Y. Chen, Y. Gao, H. Chen, D. Zeng, Y. Li, Y. Zheng, F. Li, X. Ji, X. Wang, F. Chen, Q. He, L. Zhang and J. Shi, *Adv. Funct. Mater.*, 2012, **22**, 1586-1597.
20 L. Zeng, Y. Pan, Y. Tian, X. Wang, W. Ren, S. Wang, G. Lu and A. Wu, *Biomaterials*, 2015, **57**, 93-106.
21 J. N. Liu, W. B. Bu and J. L. Shi, *Accounts Chem. Res.* 2015, **48**, 1797-1805.
22 D. Yang, P. Ma, Z. Hou, Z. Cheng, C. Li and J. Lin, *Chem. Soc. Rev.*, 2015, **44**, 1416-1448.
23 X. Zhang, F. Li, S. Guo, X. Chen, X. Wang, J. Li and Y. Gan, *Biomaterials*, 2014, **35**, 3650-3665.
24 X. Zhu, J. Zhou, M. Chen, M. Shi, W. Feng and F. Li, *Biomaterials*, 2012, **33**, 4618-4627.
25 F. Zhang, G. B. Braun, A. Pallaoro, Y. Zhang, Y. Shi, D. Cui, M. Moskovits, D. Zhao and G. D. Stucky, *Nano Lett.*, 2012, **12**, 61-67.
26 A. Li, P. Zhang, X. Chang, W. Cai, T. Wang and J. Gong, *Small*, 2015, **11**, 1892-1899.
27 L. Li, F. Tang, H. Liu, T. Liu, N. Han, D. Chen, X. Teng and J. He, *ACS Nano*, 2010, **4**, 6874-6882.
28 L. Zhao, J. Peng, M. Chen, Y. Liu, L. Yao, W. Feng and F. Li, *ACS Appl. Mater. Inter.*, 2014, **6**, 11190-11197.
29 J. Liu, Y. Liu, W. Bu, J. Bu, Y. Sun, J. Du and J. Shi, *J. Am. Chem. Soc.,* 2014, **136**, 9701-9709.
30 Y. Chen, H. Chen, S. Zhang, F. Chen, L. Zhang, J. Zhang, M. Zhu, H. Wu, L. Guo, J. Feng and J. Shi, *Adv. Funct. Mater.*, 2011, **21**, 270-278.
31 X. Kang, Z. Cheng, D. Yang, P. a. Ma, M. Shang, C. Peng, Y. Dai and J. Lin, *Adv. Funct. Mater.*, 2012, **22**, 1470-1481.
32 J. Yang, D. Shen, L. Zhou, W. Li, X. Li, C. Yao, R. Wang, A. M. El-Toni, F. Zhang and D. Zhao, *Chem. Mater.*, 2013, **25**, 3030-3037.
33 W. Zhang, Y. Wang, X. Sun, W. Wang and L. Chen, *Nanoscale*, 2014, **6**, 14514-14522.
34 Y. Zhu, T. Ikoma, N. Hanagata and S. Kaskel, *Small*, 2010, **6**, 471-478.

35 L. Zhao, J. Peng, Q. Huang, C. Li, M. Chen, Y. Sun, Q. Lin, L. Zhu and F. Li, *Adv. Funct. Mater.*, 2014, **24**, 363-371.
36 S. Lu, D. Tu, P. Hu, J. Xu, R. Li, M. Wang, Z. Chen, M. Huang and X. Chen, *Angew. Chem. Int. Ed.*, 2015, **54**, 7915-7919.
37 Y. Liu, Y. Liu, W. Bu, Q. Xiao, Y. Sun, K. Zhao, W. Fan, J. Liu and J. Shi, *Biomaterials*, 2015, **49**, 1-8.
38 J. Liu, J. Bu, W. Bu, S. Zhang, L. Pan, W. Fan, F. Chen, L. Zhou, W. Peng, K. Zhao, J. Du and J. Shi, *Angew. Chem. Int. Ed.,* 2014, **53**, 4551-4555.
39 W. Fan, B. Shen, W. Bu, F. Chen, Q. He, K. Zhao, S. Zhang, L. Zhou, W. Peng, Q. Xiao, D. Ni, J. Liu and J. Shi, *Biomaterials*, 2014, **35**, 8992-9002.
40 W. Fan, B. Shen, W. Bu, F. Chen, K. Zhao, S. Zhang, L. Zhou, W. Peng, Q. Xiao, H. Xing, J. Liu, D. Ni, Q. He and J. Shi, *J. Am. Chem. Soc.*, 2013, **135**, 6494-6503.
41 H. Qiao and Y. Zhang, *Langmuir*, 2008, **24**, 12123-12125.
42 Z. Teng, S. Wang, X. Su, G. Chen, Y. Liu, Z. Luo, W. Luo, Y. Tang, H. Ju, D. Zhao and G. Lu, *Adv. Mater.*, 2014, **26**, 3741-3747.
43 D. Ma, L. Meng, Y. Chen, M. Hu, Y. Chen, C. Huang, J. Shang, R. Wang, Y. Guo and J. Yang, *ACS Appl. Mater. Inter.*, 2015, **7**, 16257-16265.
44 G. Xing, H. Yuan, R. He, X. Gao, L. Jing, F. Zhao, Z. Chai and Y. Zhao, *J. Phys. Chem. B*, 2008, **112**, 6288-6291.
45 J. Zhou, Q. Liu, W. Feng, Y. Sun and F. Li, *Chem. Rev.,* 2015, **115**, 395-465.
46 A. Gnach, T. Lipinski, A. Bednarkiewicz, J. Rybka and J. Capobianco, *Chem. Soc. Rev.*, 2015, **44**, 1561-1584.